








## Spatial Variability of the Snowmelt-Albedo Feedback in Antarctica

### Key Points:

- We use a regional climate model to quantify the snowmelt-albedo feedback for the Antarctic ice sheet
- We find that this feedback is most active on East Antarctic ice shelves
- Precipitation frequency, timing, and summer 2 m air temperature are key parameters for its importance

C. L. Jakobs<sup>1</sup> , C. H. Reijmer<sup>1</sup> , M. R. van den Broeke<sup>1</sup> , W. J. van de Berg<sup>1</sup> , and J. M. van Wessem<sup>1</sup> 

<sup>1</sup>Institute for Marine and Atmospheric Research Utrecht, Utrecht University, Utrecht, The Netherlands

### Correspondence to:

C. L. Jakobs,  
[c.l.jakobs@uu.nl](mailto:c.l.jakobs@uu.nl)

### Citation:

Jakobs, C. L., Reijmer, C. H., van den Broeke, M. R., van de Berg, W. J., & van Wessem, J. M. (2021). Spatial variability of the snowmelt-albedo feedback in Antarctica. *Journal of Geophysical Research: Earth Surface*, 126, e2020JF005696. <https://doi.org/10.1029/2020JF005696>

Received 27 MAY 2020  
 Accepted 22 DEC 2020

**Abstract** Surface melt is an important process for the stability of ice shelves, and therewith the Antarctic ice sheet. In Antarctica, absorption of solar radiation is mostly the largest energy source for surface melt, which is further enhanced by the snowmelt-albedo feedback (SMAF): Refrozen snow has a lower albedo than new snow, which causes it to absorb more solar radiation, further increasing the energy available for surface melt. This feedback has previously been shown to increase surface melt by approximately a factor of 2.5 at Neumayer Station in East Antarctica. In this study, we use a regional climate model to quantify SMAF for the entire Antarctic ice sheet. We find that it is most effective on ice shelves in East Antarctica, and is less important in the Antarctic Peninsula and on the Ross and Filchner-Ronne ice shelves. We identify a relationship between SMAF and average summer 2 m air temperatures, and find that SMAF is most important around  $265 \pm 2$  K. On a subseasonal scale, we identify several parameters that contribute to SMAF: the length of dry periods, the time between significant snowfall events and snowmelt events, and prevailing temperatures. We then apply the same temperature dependency of SMAF to the Greenland ice sheet and find that it is potentially active in a narrow band around the ice sheet, and finally discuss how the importance of SMAF could change in a warming climate.

**Plain Language Summary** The Antarctic ice sheet is surrounded by ice shelves: floating extensions that prevent it from flowing into the oceans. The stability of these ice shelves is mainly affected by the melting of snow and ice, leading to a potential disintegration of the entire ice shelf. To properly simulate the climate, models should therefore be able to accurately reproduce snowmelt rates. Snowmelt in Antarctica is mainly driven by the absorption of solar radiation. This is subject to a positive feedback: when snow melts, it becomes darker, causing it to absorb more radiation. This leads to more energy that is available for snowmelt, which further darkens the surface. In this study, we use a climate model to quantify the importance of this feedback for the Antarctic ice sheet. We find that it is most important in regions with an average summer 2 m air temperature around 265 K. We furthermore find that during a long, dry period in summer, the feedback is more effective, and that the timing between snowfall and snowmelt partly determines how much the feedback will affect snowmelt. As a final step, we estimate how important this feedback is in Greenland, and how the observed patterns could change in a warming climate.

## 1. Introduction

The Antarctic ice sheet (AIS) contains approximately 26 million km<sup>3</sup> of ice, equivalent to a global mean sea level change of 58 m (Morlighem et al., 2020). Ice shelves, the floating extensions of the grounded ice sheet, are present along ~74% of the AIS (Bindschadler et al., 2011), buttressing ice flow of the grounded ice sheet. In recent years, gravity observations, altimetry and ice velocity observations from space, combined with snowfall data from regional climate models, show that mass loss from the AIS has been accelerating: Shepherd et al. (2018) report a mass loss rate of  $109 \pm 56$  Gtyr<sup>-1</sup> over the period 1992–2017. Both ice-shelf thinning and break-up have been associated with the acceleration of its feeding glaciers (Rott et al., 2011; Scambos et al., 2004), causing the high mass loss rates in coastal West Antarctica and the Antarctic Peninsula (AP) (Turner et al., 2017; Wouters et al., 2015). The biggest mass loss is observed in West Antarctica, as a result of the thinning of ice shelves, which experience enhanced basal melt through increased ocean-ice heat exchange (Massom et al., 2018; Pritchard et al., 2012). On the west side of the AP, break-up events on Wilkins ice shelf have also been associated with increased basal melt rates, leading to changes in buoyant

© 2021. The Authors.

This is an open access article under the terms of the [Creative Commons Attribution](https://creativecommons.org/licenses/by/4.0/) License, which permits use, distribution and reproduction in any medium, provided the original work is properly cited.

forces (Braun et al., 2009; Padman et al., 2012). Many ice shelves in Antarctica also experience surface melt by energy exchange at the atmosphere-ice-shelf interface (Kingslake et al., 2017). The recent collapse of Larsen A and B ice shelves on the east side of the AP was preceded by extensive surface melt, inducing firn saturation, meltwater ponding, and hydrofracturing (Glasser & Scambos, 2008; Van den Broeke, 2005). Ice-shelf stability is thus crucial for the future mass balance of the AIS. Because both basal and surface melt are expected to increase in a warming climate also for the colder ice shelves (Trusel et al., 2015), a proper representation of ice-shelf melt processes is essential in climate modeling.

In this study, we focus on surface melt processes. Weather stations, satellites, and climate models have been used to estimate surface melt rates on Antarctic ice shelves (Agosta et al., 2019; Bromwich et al., 2013; Souverijns et al., 2019; Trusel et al., 2015; Van Kampenhout et al., 2017; Van Wessem et al., 2018). In situ observations show that in the cold climate of Antarctica, melt is often intermittent and insolation is usually the most important energy source for surface melt (Jonsell et al., 2012; King et al., 2015; Reijmer et al., 2005; Van den Broeke et al., 2005a), which also explains why temperature-index models do not work well in these regions (Jakobs et al., 2020). The absorption of solar radiation is in turn enhanced by the snowmelt-albedo feedback (SMAF; Jakobs et al., 2019): when snow melts, meltwater percolates into the subsurface snow layers where it can refreeze. As refrozen snow consists of larger snow grains than new snow, it reduces the backward scattering of photons (Wiscombe & Warren, 1980), i.e., it has a lower albedo. As a result, the surface absorbs more incoming solar radiation, leading to more surface melt, representing a positive feedback. Therefore, it is crucial for climate models to use a snow albedo parameterization that includes this melt-albedo feedback when modeling surface melt on the AIS (Alexander et al., 2019; Cullather et al., 2014; Van Dalum et al., 2019).

In a previous study, we used high-quality meteorological observations from Neumayer Station, located on Ekström ice shelf in East Antarctica, to quantify the effect of SMAF on surface melt rates (Jakobs et al., 2019). We used a surface energy balance (SEB) model that includes a grain-size-dependent albedo parameterization, and found that on average, SMAF enhanced surface melt (1992–2016) at Neumayer Station by a factor of 2.5, but with significant inter-annual variability. The current study aims to extend our previous work to the entire AIS, using the regional atmospheric climate model (RACMO2). This climate model is specifically developed to simulate polar climates and has been extensively evaluated using observations from automatic weather stations, including melt rates (Jakobs et al., 2020; Van Wessem et al., 2018). Its albedo parameterization and ability to represent the near-surface Antarctic climate and surface mass balance make it well-suited to study SMAF at the continental scale (Van Wessem et al., 2018). It is important to note that, because SMAF represents the ratio between a “real” and an “imaginary” melt amount, its value can only be modeled and cannot be directly compared to observations. Only one component of SMAF, the “real” melt, can be compared to observations, which has been done in Jakobs et al. (2019).

In the next section, we introduce the climate model RACMO2 and describe the albedo parameterization used. In Section 3, we present a map of SMAF in Antarctica (Section 3.1), discussing its spatial variability as well as the inter-annual variability at different locations (Section 3.2). We identify regions in Antarctica that are most affected by SMAF (Section 3.3) and present local case studies on a daily timescale to identify conditions where SMAF is largest (Section 3.4). In Section 4, we summarize our findings about SMAF, comment on the potential importance of SMAF in Greenland, and how SMAF will affect surface melt in the future on both ice sheets.

## 2. Methods

### 2.1. Model Descriptions

The regional climate model RACMO2 is developed by the Royal Netherlands Meteorological Institute (RSMI). It is a hydrostatic model that combines the dynamical core of the High Resolution Limited Area Model (HIRLAM; Undén et al. (2002)) with the physics parameterizations of the Integrated Forecast System (IFS, version CY33r1) of the European Centre for Medium-Range Weather Forecast (ECMWF) (ECMWF, 2009).

For this study, we use the latest polar version (RACMO2.3p2, from now on referred to as RACMO2), which has been specifically developed for use over glaciated regions (Reijmer et al., 2005; Van Wessem et al., 2018). The atmosphere is represented by 40 vertical levels and the model is forced by the ERA-Interim reanalysis product at its lateral boundaries as well as in the upper atmosphere and at the ocean surface (Van de Berg & Medley, 2016). The atmospheric component is coupled to a multilayer snow model (Ettema et al., 2010), which allows for meltwater percolation, refreezing, and runoff. Furthermore, RACMO2 uses an albedo parameterization that depends on grain size (Gardner & Sharp, 2010; Kuipers Munneke et al., 2011) and a drift-*ing*-snow scheme that simulates horizontal transport of snow by near-surface winds (Lenaerts et al., 2012).

The snow model typically uses 30–50 layers and is initialized using the firn pack from a run with a firn densification model (Van Wessem et al., 2018). The uppermost layer embeds the fresh-snow layer of which the density and grain size evolution are treated separately. Layers are merged with the layer below if their thickness becomes less than half the ideal thickness for their depth. For the surface layer, merging occurs if the thickness is less than 3.3 cm. If the surface layer becomes thicker than 8.7 cm, it is split. Unless the original fresh snow layer is thinner than 3.3 cm, the new upper layer contains fresh snow only. All other layers are split in two equal parts if they become thicker than twice the ideal thickness for their depth. If the firn/ice column becomes thinner than 30 m, the lowermost layer is duplicated.

Van Wessem et al. (2018) compared the output of RACMO2 with in situ measurements of surface temperature, radiation fluxes, turbulent fluxes, and wind speed. They found that RACMO2 yields reliable estimates of surface temperatures and net short-wave radiation ( $R^2 = 0.94$ ; bias =  $-2.2 \text{ W m}^{-2}$ ), and performs adequately in modeling turbulent fluxes, net long-wave radiation and wind speed. They furthermore found a good correlation of surface melt rates with the results from the QuikSCAT satellite. Jakobs et al. (2020) showed that RACMO2 reproduces surface melt rates with reasonable accuracy: compared to in situ melt estimates from (automatic) weather stations in the AP and Dronning Maud Land, RACMO2 slightly underestimates surface melt rates (bias =  $-7.3 \text{ mm w. e. yr}^{-1}$ ) but overall, the agreement is good ( $R^2 = 0.83$ ).

RACMO2 solves the Surface Energy Balance (SEB) equation, which describes the energy exchange between the surface, the subsurface, and the atmosphere and determines the amount of energy available for surface melt:

$$M = R_{\text{net}} + Q_S + Q_L + Q_G, \quad (1)$$

where  $R_{\text{net}}$  is the net radiation, the sum of net short-wave and net long-wave radiation,  $Q_S$  and  $Q_L$  are the turbulent fluxes of sensible and latent heat, respectively, and  $Q_G$  is the surface value of the subsurface heat flux.  $M$  is the energy available for surface melt, which is equal to 0 when the surface temperature is below the melting point of ice (273.15 K). In an iterative procedure, the surface temperature is determined so that the SEB is closed. If this temperature would exceed 273.15 K, it is forced to this value and excess energy is available for surface melt. The turbulent fluxes  $Q_S$  and  $Q_L$  are determined using Monin-Obukhov similarity theory, which relates the fluxes to the near-surface gradients of wind speed, potential temperature and humidity (see e.g., Van den Broeke et al., 2005b). The subsurface heat flux  $Q_G = k \frac{\partial T}{\partial z}$ , where  $k$  is the effective thermal conductivity of the snow/ice and  $\frac{\partial T}{\partial z}$  the temperature gradient in the near-surface snowpack. The snow model solves the heat-conductivity equation to obtain the sub-surface temperature profile and there-with  $Q_G$  (Ettema et al., 2010):

$$\rho c_p \frac{\partial T}{\partial t} = -\frac{\partial}{\partial z} \left( k \frac{\partial T}{\partial z} \right) + q_{\text{refr}}, \quad (2)$$

where  $q_{\text{refr}}$  is the energy released by the refreezing of meltwater per unit time per area,  $\rho$  is the snow density and  $c_p$  is the specific heat capacity. Note that Equation 2 does not include a term describing penetration of short-wave radiation, since it is not considered in the used model version. Short-wave radiation penetration will be implemented in the future version RACMO2.3p3 (Van Dalum et al., 2020).

In this study, we used RACMO2.3p2, which adopts the albedo parameterization of Gardner and Sharp (2010), in which the albedo is described as a base value  $\alpha_s$  with modifications due the solar zenith angle  $\theta$  ( $d\alpha_u$ ),

the cloud optical thickness  $\tau$  ( $d\alpha_\tau$ ), the concentration of black carbon in the snow ( $d\alpha_c$ ), and surface elevation ( $d\alpha_h$ ; Kuipers Munneke et al., 2011). The base albedo  $\alpha_s$  for each snow layer is given by Gardner and Sharp (2010):

$$\alpha_s = 1.48 - 1.27048r_e^{0.07}, \quad (3)$$

where  $r_e$  is the snow grain size in meters, in turn parameterized as

$$r_e(t) = \left[ r_e(t-1) + dr_{e,dry} + dr_{e,wet} \right] f_o + r_{e,0} f_n + r_{e,r} f_r, \quad (4)$$

where  $dr_{e,dry}$  and  $dr_{e,wet}$  describe grain growth due to dry and wet snow metamorphism, respectively. With  $r_{e,0}$  and  $r_{e,r}$  we denote the grain sizes of new and refrozen snow, set to constant values of  $r_{e,0} = 54 \cdot 10^{-6}$  m (Kuipers Munneke et al., 2011) and  $r_{e,r} = 1 \cdot 10^{-3}$  m (Van Wessem et al., 2018). The choice of fresh snow grain size is limited by the availability of look-up tables for the dry snow metamorphism  $dr_{e,dry}$  (see also Jakobs et al. (2019)); the refrozen snow grain size provided the best comparison with observations (Van Wessem et al., 2018). Furthermore,  $f_o$ ,  $f_n$ , and  $f_r$  are the fractions of old, fresh and refrozen snow. The values of  $f_o$ ,  $f_n$ , and  $f_r$  are all between 0 and 1, and  $f_r$  can only be non-zero for the fresh snow layer. The effect on albedo of the older snow below the fresh snow in the top model layer is estimated by

$$\alpha'_s = \left( \alpha_s^{\text{old}} - \alpha_s^{\text{fsh}} \right) + A \left( \alpha_s^{\text{fsh}} - \alpha_s^{\text{old}} \right), \quad (5)$$

where “fsh” and “old” indicate the fresh snow layer and the older snow, respectively, and  $A$  is a factor depending on  $\alpha_s^{\text{fsh}}$  and layer thickness  $z$ . If no fresh snow layer is present, the upper two model layers are used for Equation 5. This approach is different from Kuipers Munneke et al. (2011) and Jakobs et al. (2019), who used more than two layers to calculate the surface albedo. Equations for  $d\alpha_u$ ,  $d\alpha_\tau$ ,  $dr_{e,dry}$ ,  $dr_{e,wet}$  and  $A$  can be found in Gardner and Sharp (2010). In the Results section, time series of resulting albedo values are discussed for various climate zones in Antarctica.

The impact of snow impurities is assumed negligible for Antarctica and thus we set  $d\alpha_c = 0$  (Bisiaux et al., 2012; Grenfell et al., 1994; Marquetto et al., 2020; Warren & Clarke, 1990). Jakobs et al. (2020) and Van Wessem et al. (2018) showed that with these settings RACMO2.3p2 faithfully reproduces Antarctic snow albedo, net short-wave radiation and snowmelt fluxes.

## 2.2. Quantifying SMAF

To quantify the effect of SMAF, we performed two simulations with RACMO2 on a 27 km horizontal resolution for the period 1979–2018: a baseline run  $R_0$  in which the full albedo parameterization is used as described above, and a sensitivity run  $R_1$ , in which the contribution of refrozen snow to snow grain size, and hence surface albedo, is disabled by setting  $f_r = 0$  in Equation 4. The same approach was used by Jakobs et al. (2019) to quantify SMAF at Neumayer Station in East Antarctica. The term “period-average” is used throughout this article, referring to the period 1979–2018.

There are several ways to quantify SMAF. The most robust definition is  $\text{SMAF}_t$ , the ratio of the total (“t”) cumulative amounts of surface melt in  $R_0$  and  $R_1$  over the entire period available (in this study 1979–2018). We use this measure to interpret the spatial variability of SMAF and e.g., its correlation with period-average temperature. SMAF can also be determined on a seasonal (“s”) basis, i.e. the ratio of seasonal (in this study July–June) melt in  $R_0$  and  $R_1$ , and is denoted by  $\text{SMAF}_s$ . Time series of  $\text{SMAF}_s$  are used to study the inter-annual variability of SMAF and the connection to the SEB. Since SMAF is defined over snow, we do not consider the melt occurring on blue ice areas, where sublimation and erosion by drifting snow cause surface mass balance to be negative and dark glacier ice is exposed (Lenaerts et al., 2018).

In this study, it was decided to only include the first-order effect of refreezing on grain size and albedo ( $f_r = 0$  in Equation 4), and not the effects of meltwater ponding and wet snow metamorphism. Wet snow metamorphism rate depends non-linearly on liquid water content (LWC), which represents meltwater that did

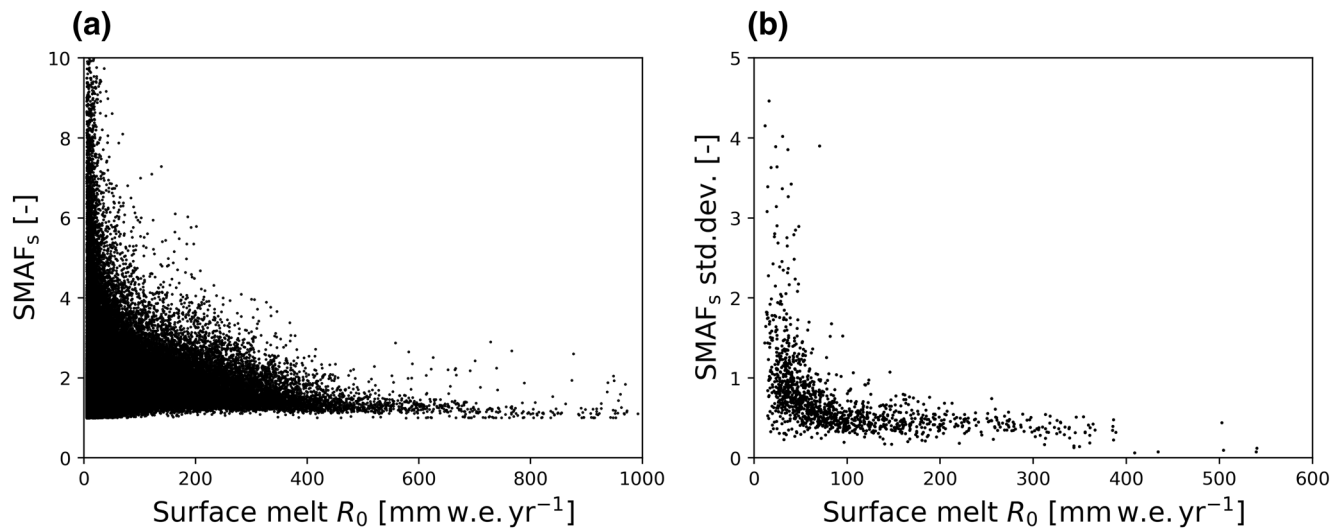


**Figure 1.** (a) Relationship between surface melt rate and SMAF<sub>s</sub>. Each dot represents one season with at least 5 mm w.e. for all grid points within the model domain. (b) Period-average annual surface melt versus SMAF<sub>s</sub> standard deviation for all grid points with period-average annual surface melt  $\geq 5$  mm w.e.

not refreeze after percolating in the snow. Most RCMs, including RACMO2.3p2, only consider irreducible water that is retained through capillary forces, and not e.g., the formation of ponds through standing water on semi-impermeable ice lenses and/or lateral water transport. For the current RACMO2.3p2 settings (LWC maximized at 2% of the available pore space), the effect of ignoring wet snow metamorphism on SMAF is small for a wide range of Antarctic climate conditions (0.1%–4%, based on the AWS locations in Jakobs et al. (2019)). That is why quantifying the effects of wet snow metamorphism and meltwater ponding on SMAF is postponed until these processes are known with greater certainty.

### 3. Results

#### 3.1. Spatial Distribution of SMAF

Since SMAF is defined as the ratio of surface melt in two different runs, we first present the relation between annual surface melt rates and SMAF<sub>s</sub> in Figure 1a, for seasons with at least 5 mm w.e. of surface melt, for each model grid cell. The figure shows that the highest SMAF<sub>s</sub> values occur in low-melt regions, while in high-melt regions SMAF<sub>s</sub> is close to 1. It furthermore shows that melt is not the only driver of SMAF<sub>s</sub>. In this section we study the spatial distribution of SMAF and surface melt; in Section 4, we then discuss possible other drivers of SMAF.

To identify the regions where SMAF is most important, we first need to know the spatial distribution of surface melt in Antarctica. This is presented in Figure 2a, with the highest values occurring on both sides of the AP, locally exceeding 300 mm w.e. yr<sup>-1</sup>. Extreme values ( $>500$  mm w.e. yr<sup>-1</sup>) occur on small islands north of the AP. The highest surface melt rates in East Antarctica are found on Shackleton ice shelf (indicated in Figure 2c with an "S"), due to its northerly location. The lowest values are found on the Ross and Filchner-Ronne ice shelves. The absolute increase in seasonal average melt because of SMAF ( $R_0 - R_1$ ) is shown in Figure 2b. A pattern similar to Figure 2a emerges, with the highest values in the AP and on Shackleton ice shelf, but also in coastal Dronning Maud Land and the Amundsen Sea sector. When integrated over the entire ice sheet, including SMAF increases the annual melt from 70 Gt yr<sup>-1</sup> in  $R_1$  to 116 Gt yr<sup>-1</sup> in  $R_0$ , i.e., an increase of 46 Gt yr<sup>-1</sup> (+65%).

Figure 2c shows the resulting SMAF<sub>s</sub>, ranging from 1 to  $\sim 2.8$ , for locations with at least 5 mm w.e. of period-average seasonal surface melt. The highest values are found in coastal Dronning Maud Land and the Amundsen Sea sector; these locations have relatively low seasonal surface melt rates, combined with an increase because of SMAF that is relatively large. Lower values are found in low-melt regions such as on the



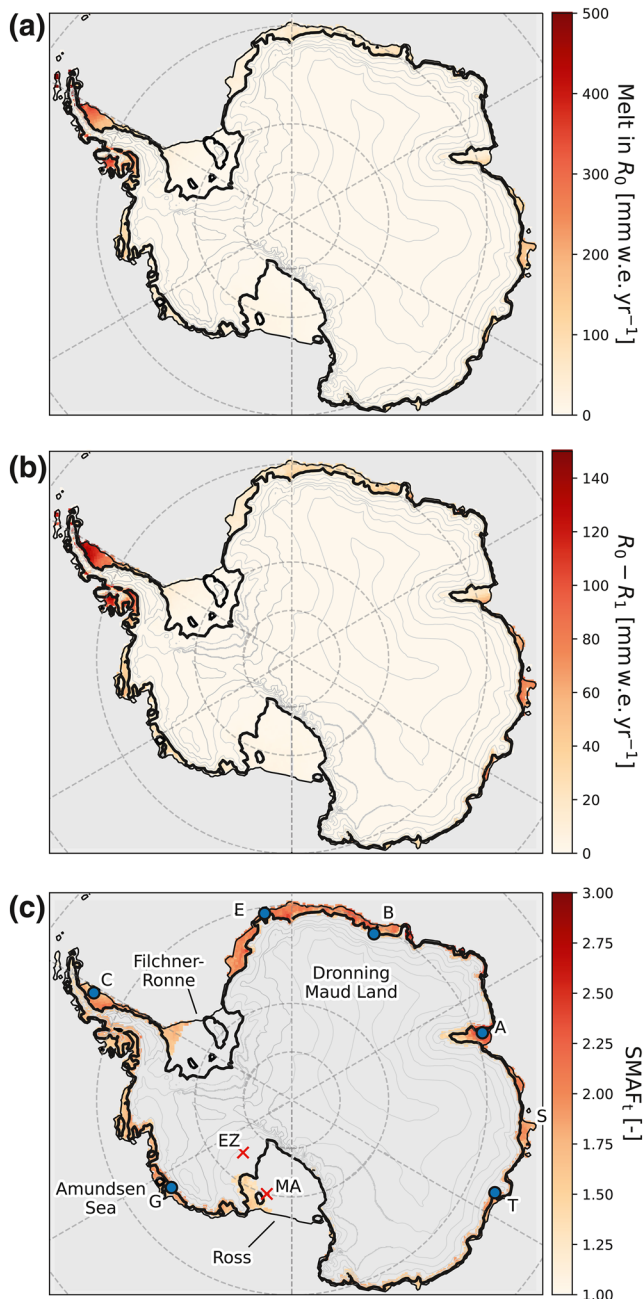


**Figure 2.** (a) Period-average seasonal surface melt rates modeled by RACMO2, with the full albedo parameterization (run  $R_0$ ). (b) Difference in average seasonal surface melt rates between runs  $R_0$  and  $R_1$ . (c)  $\text{SMAF}_I$  for all grid points with period-average seasonal surface melt  $\geq 5$  mm w.e. Blue dots indicate sites for which Figure 3 presents time series of surface melt: Ekström (e), King Baudouin (b), Amery (a), Totten (T), Getz (g), and Larsen C (c) ice shelves. Red crosses indicate the sites for which daily values of SEB components and meteorological variables are presented in Figure 9, Shackleton ice shelf is indicated with an S.

Ross and Filchner-Ronne ice shelves, and high-melt regions such as the northern AP. These patterns are discussed in more detail in Section 3.3, but first we consider the temporal variability of  $\text{SMAF}_s$ .

### 3.2. Temporal Variability of $\text{SMAF}$

For six locations, indicated by blue dots in Figure 2c, time series of seasonal snowmelt for both runs ( $R_0$  and  $R_1$ ) are presented in Figure 3. The ratio between these two yields the seasonal  $\text{SMAF}_s$  value; indicated in top-right are  $\text{SMAF}_I$  and the average and standard deviation of  $\text{SMAF}_s$ . The average of  $\text{SMAF}_s$  is greater than  $\text{SMAF}_I$ ; this is a result of the lower limit of  $\text{SMAF}_s$ , which is by definition 1. Especially in low-melt regions, summers with high  $\text{SMAF}_s$  have a larger effect on its average than on  $\text{SMAF}_I$ .

These locations were selected to illustrate the different  $\text{SMAF}$  regimes. On Larsen C ice shelf (Figure 3f),  $\text{SMAF}$  leads to an increase in surface melt by a relatively constant factor every year, characterized by a low standard deviation of  $\text{SMAF}_s$ . This is different from, e.g., Amery ice shelf (Figure 3c), where  $\text{SMAF}_s$  varies strongly from year to year (high standard deviation of  $\text{SMAF}_s$ ). For the other locations, the standard deviation ranges between these extremes. Note that Larsen C and King Baudouin ice shelves have significant melt events outside of the summer months, because of regular Föhn events (Lenaerts et al., 2017; Wiesenekker et al., 2018). These are however not sensitive to  $\text{SMAF}$ , as they are not driven by short-wave radiation but rather by turbulent heat fluxes as well as exposure of bare ice through snow erosion.

Figure 1b shows a decrease of  $\text{SMAF}_s$  inter-annual variability with increasing melt. In low-melt regions ( $< 100$  mm w.e. yr $^{-1}$ ), melt is highly intermittent and the albedo remains generally high. If melt occurs, the albedo decreases significantly and surface melt increases relatively strongly, yielding large  $\text{SMAF}_s$  values. In contrast, high-melt regions have a lower surface albedo to start with due to the higher prevailing temperatures; the albedo-lowering effect of melt is therefore less influential and melt is only slightly enhanced, leading to low  $\text{SMAF}_s$  values and variability.

Figures 1 and 2 present the relationship between surface melt and  $\text{SMAF}$ . However, these figures also suggest there are more drivers determining  $\text{SMAF}$ . These are the subject of Section 3.3, where we identify climatic regions where  $\text{SMAF}$  is most active. Section 3.4 focuses on how  $\text{SMAF}$  is related to the SEB on a daily timescale, for different regimes.

### 3.3. Climatic Drivers of $\text{SMAF}$

To understand the spatial patterns in Figure 2c, we investigated the relationship between  $\text{SMAF}_I$  and several quantities: summer (November–February) 2 m air temperature, summer precipitation and seasonal surface melt rate. The most discernible pattern is observed in the correlation with temperature, which is therefore used below to describe large-scale climate drivers of  $\text{SMAF}_I$ . Precipitation and surface melt are used to discuss  $\text{SMAF}$  on a subseasonal scale in Section 3.4.

Figure 4 shows that the highest  $\text{SMAF}_I$  values are found in regions with an average summer 2 m air temperature of  $\sim 265$  K (defined as  $T_c$ ), where  $\text{SMAF}_I$  reaches an average value of 1.9. This pattern is not very

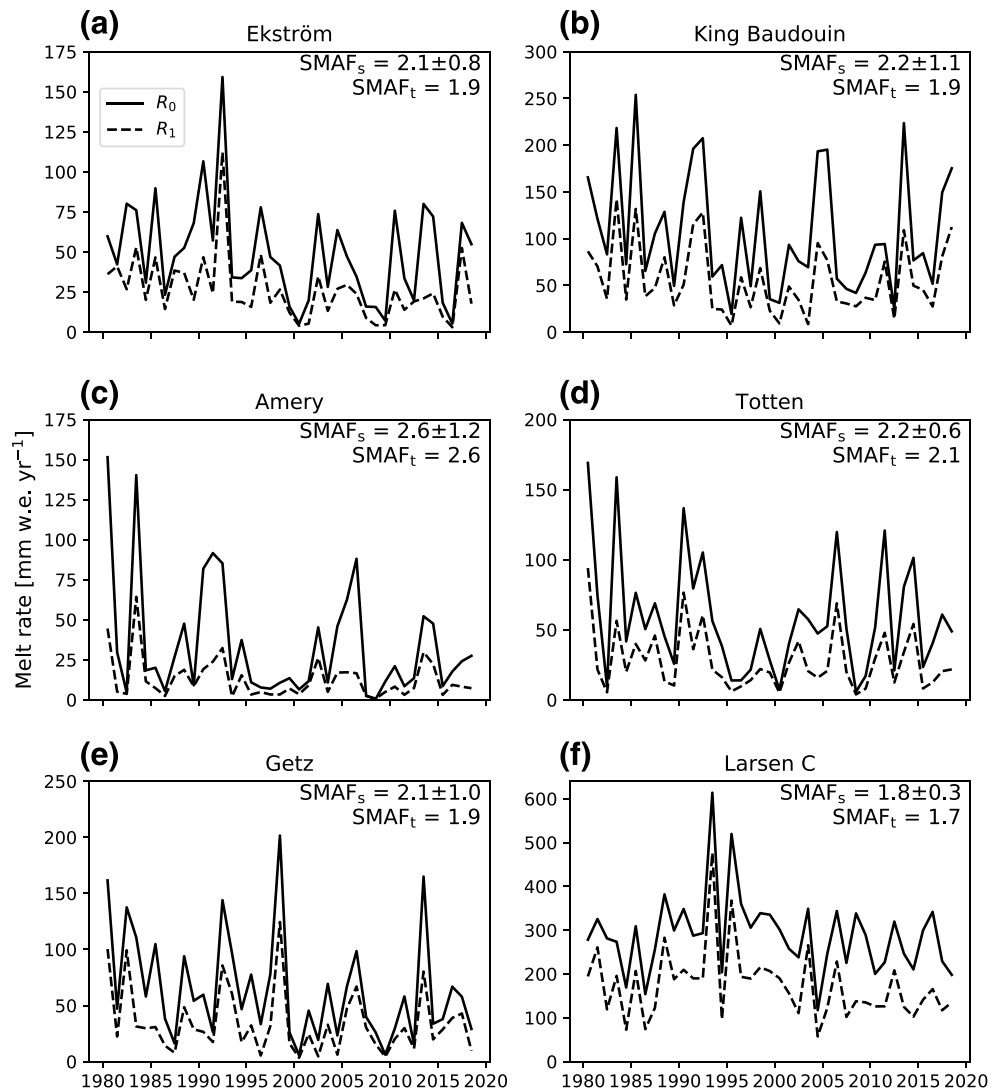


**Figure 3.** Time series of seasonal surface melt rates at various ice shelves around the Antarctic ice sheet (see Figure 2c). Melt in  $R_0$  is indicated with a solid line, in  $R_1$  with a dashed line; the ratio between the two gives the seasonal  $SMAF_s$  value. Numbers in the top right corner are  $SMAF_t$ , the average of  $SMAF_s$  and its standard deviation.

sensitive to the chosen period; it is similar if the time period is limited to an arbitrary 10-year or 20-year period throughout the total period (not shown). Its shape suggests a “peak bandwidth” rather than a single peak value. Therefore, in the following, we consider a 2 K bandwidth around  $T_c$ , i.e.,  $T_c = 265 \pm 2$  K.

In regions with temperatures above or below  $T_c$ ,  $SMAF_t$  gradually decreases to 1. In the colder regions ( $T < 263$  K), surface melt rates are generally low (mostly  $< 30$  mm w. e.  $yr^{-1}$ ) and  $SMAF$  only moderately enhances surface melt ( $\sim 40\%–50\%$ ). In warmer regions ( $T > 267$  K), such as the AP,  $SMAF$  is also less important for surface melt; due to the relatively mild conditions, the contribution of turbulent heat fluxes is more important to melt energy than absorption of short-wave radiation. This causes melt events that are less affected by the surface albedo, limiting the influence of  $SMAF$ . This is discussed in more detail in Section 3.4.

Figure 5 shows large negative departures from  $T_c$  on the Ross, Filchner-Ronne and Amery ice shelves, which extend far to the south and are the coldest areas which experience surface melt in Antarctica, with average summer 2 m air temperatures of 260 K and lower. These ice shelves represent the left tail of the temperature- $SMAF_t$  relation (Figure 4), where  $SMAF$  has a limited effect on surface melt rates. The AP is the warmest region of Antarctica, with average summer 2 m air temperatures of 270 K and higher. It is located

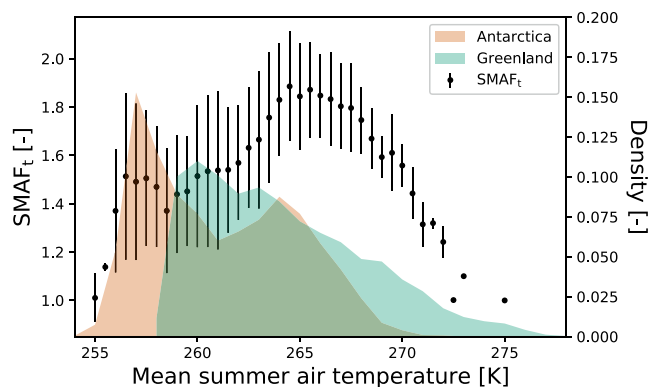


**Figure 4.**  $SMAF_t$  as a function of binned (0.5 K) November–February average 2 m air temperature for all grid points with period-average seasonal surface melt of at least 5 mm w.e. (black dots, lines indicate the standard deviation; the three rightmost dots have no lines because there is only one data point within the temperature bin). *Right axis:* The shading indicates the normalized distribution of average summer 2 m air temperature for all grid points with period-average seasonal surface melt of at least 5 mm w.e. in Antarctica (orange, November–February) and in Greenland (green, accumulation zone only, May–August; Noël et al. (2018)). Only Greenland accumulation area values are shown, as  $SMAF$  is undefined over the ablation area. In Antarctica, only very few points in RACMO2 are ablation area, and these points are modeled in non-melt areas, so do not impact the analysis.

in the right tail of the temperature– $SMAF_t$  relation, where surface melt is semi-continuous, mainly driven by high 2 m air temperatures, and  $SMAF$  is also of limited importance for surface melt rates.

The remaining, smaller ice shelves in East and West Antarctica experience average summer 2 m air temperatures around  $T_c$ , displayed in white in Figure 5a, with the 2 K bandwidth indicated with black dots. This indicates that  $SMAF$  is currently significantly ( $\sim$ doubling) enhancing surface melt on ice shelves all around the AIS. In this high- $SMAF$  regime, surface melt is an intermittent process; the meteorological circumstances that favor  $SMAF$  are identified in the next section.

### 3.4. $SMAF$ and its Connection to the SEB

To investigate  $SMAF$  and its drivers more closely, we compare summers with different  $SMAF$  values at three locations: King Baudouin ice shelf, Larsen C ice shelf and Amery ice shelf (see Figure 2c for locations). These locations were selected because they represent different  $SMAF$  regimes: Moderate temperature, strong  $SMAF$  (King Baudouin; Figure 6), high temperature, weak  $SMAF$  (Larsen C, Figure 7), and low temperature, strong  $SMAF$  (Amery; Figure 8). Finally, we turn to Margaret and Elizabeth stations, on Ross ice shelf and in Marie Byrd Land, respectively, to discuss the effect of atmospheric rivers on  $SMAF$  (Figure 9).

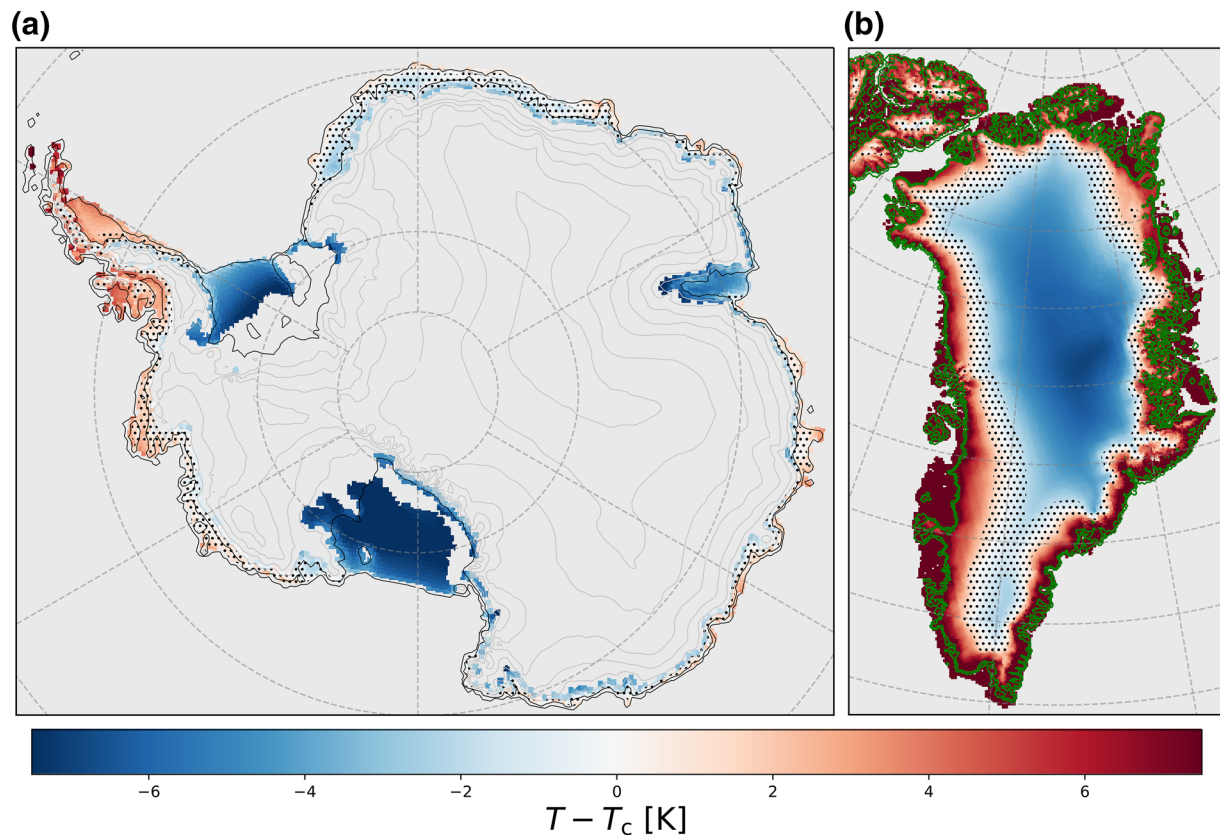
Figure 6 shows melt-season time series for a location on King Baudouin ice shelf, located in coastal Dronning Maud Land (indicated by “B” in Figure 2c), in a moderate-temperature, strong- $SMAF$  region (Figure 5a).

Figure 3b shows that in this location,  $SMAF_s$  experiences a large inter-annual variability. Figure 6 shows daily cumulative surface melt (a),(e), precipitation (b),(f), the SEB components (c),(g) and temperature and albedo (d),(h) for experiments  $R_0$  and  $R_1$  (see Section 2.2). In the melt season 2002–2003, around 15 December, a melt episode occurs immediately after a strong precipitation event (Figures 6a and 6b). Because of refreezing, the albedo drops from 0.9 to  $\sim$ 0.75 (Figure 6d). As no more significant snowfall events follow, the albedo remains low for the remainder of the season, resulting in significantly elevated  $SW_{net}$  values (Figure 6c) and a prolonged period of surface melt in  $R_0$ . The surface albedo is not reset to that of new snow until the end of the melt season. As grain growth by refreezing is inactive in  $R_1$ , the decrease in albedo after the melt event is smaller; it stabilizes at  $\sim$ 0.82. As the surface now reflects more solar radiation,  $SW_{net}$  is significantly lower and melt ceases after the first melt event following the precipitation event. In  $R_0$  melt totaled  $\sim$ 70 mm w.e. during this season, while in  $R_1$  it totaled only 8 mm w.e., yielding a high  $SMAF_s$  value of 8.5 (Figure 6a).

At the same location but two seasons later (2004–2005), a similar dry period occurred (Figures 6e–6h). Contrary to 2002–2003, melt did not start immediately after the last significant snowfall event. Rather, the albedo decreases steadily because of dry snow metamorphism in both  $R_0$  and  $R_1$ . Before the first melt of the season, the albedo had decreased to  $\sim$ 0.82 in both runs. Similar to 2002–2003, the albedo decreases more in  $R_0$  than in  $R_1$  during the melt event. However, the effect of  $SMAF$  is now less pronounced than in 2002–2003 because the albedo was already lowered, making the additional contribution of refrozen snow less important. The difference in  $SW_{net}$  is therefore also smaller, as well as the difference in surface melt rates throughout the season. The total 2004–2005 surface melt amounts are  $\sim$ 200 mm w.e. in  $R_0$  and  $\sim$ 80 mm w.e. in  $R_1$ , giving a  $SMAF_s$  of 2.5 (Figure 6e).

Larsen C ice shelf in the AP (location indicated by “C” in Figure 2c) experiences relatively high surface melt rates and higher temperatures than King Baudouin ice shelf (Figure 7), due to its more northerly location. Melt is enhanced by  $SMAF$  most efficiently between December 15, 2007 and January 1, 2008, during a prolonged dry period (Figures 7e and 7f). The subsequent difference in albedo (Figure 7h) resulted in significantly more absorption of solar radiation during this period (Figure 7g) while temperatures were high





**Figure 5.** Temperature deviation from  $T_c \equiv 265$  K, the temperature at which SMAF plateaus (see Figure 4), for Antarctica (a) and Greenland (b). Blue areas indicate regions where SMAF will become increasingly important when 2 m air temperatures rise. White areas indicate regions where SMAF is now enhancing surface melt the most. Red areas indicate regions where 2 m air temperatures/melt are too high for an optimal SMAF. Black dots indicate the 2 K bandwidth around  $T_c$ , the green contour in (b) indicates the ice sheet margin (Noël et al., 2018).

enough to sustain surface melt. The absence of such a dry period in 2002–2003 prevented SMAF from affecting surface melt as efficiently. Furthermore, the 2 m air temperature is close to the melting point throughout the season, which allowed sustained surface melt in both  $R_0$  and  $R_1$  runs. In the end, SMAF enhanced surface melt by only  $\sim 30\%$  compared to  $\sim 140\%$  in 2007–2008, which again underlines the importance of dry periods for the effectiveness of SMAF. The effect is considerably smaller than on King Baudouin ice shelf (Figure 6) because of the higher temperature on Larsen C, which allows for surface melt to proceed even in the absence of SMAF ( $R_1$ ). This also explains the smaller inter-annual variability that is observed in Figure 3f. The selected location is in the interior of Larsen C ice shelf. Figure 2 seems to suggest that SMAF increases from the ice shelf interior toward the AP mountains, likely indicative of the drier climate closer to the mountain foot owing to more frequent Föhn events.

Figure 8 shows that Amery ice shelf, East Antarctica (indicated by “A” in Figure 2c), experiences relatively low average temperatures for its latitude. The first season (panels a–d) represents the high-SMAF summer 2004–2005 without a prolonged dry period; even the precipitation event on December 30 was not able to sufficiently reset the surface albedo. During this event, melt continued because of the persistent high temperature and with it high  $Q_s$ . As a result, the new snow was quickly removed from the surface. The difference in  $SW_{net}$  in the following days is sufficient to cause high  $SMAF_s$ . In the summer of 2005–2006 (panels e–h) an even higher  $SMAF_s$  occurs, resulting from a long dry episode. A remarkably large difference in 2 m air temperature is observed (Figure 8h) during the persistent melt episode in  $R_0$  which is absent in  $R_1$ . This is caused by persistently higher surface temperatures, following larger  $SW_{net}$  and refreezing.

For the final case study, we consider the 2015–2016 melt season on Elizabeth (519 mASL) and Margaret (67 m ASL) stations, in Marie Byrd Land and on Ross ice shelf, respectively (indicated with “MA” and

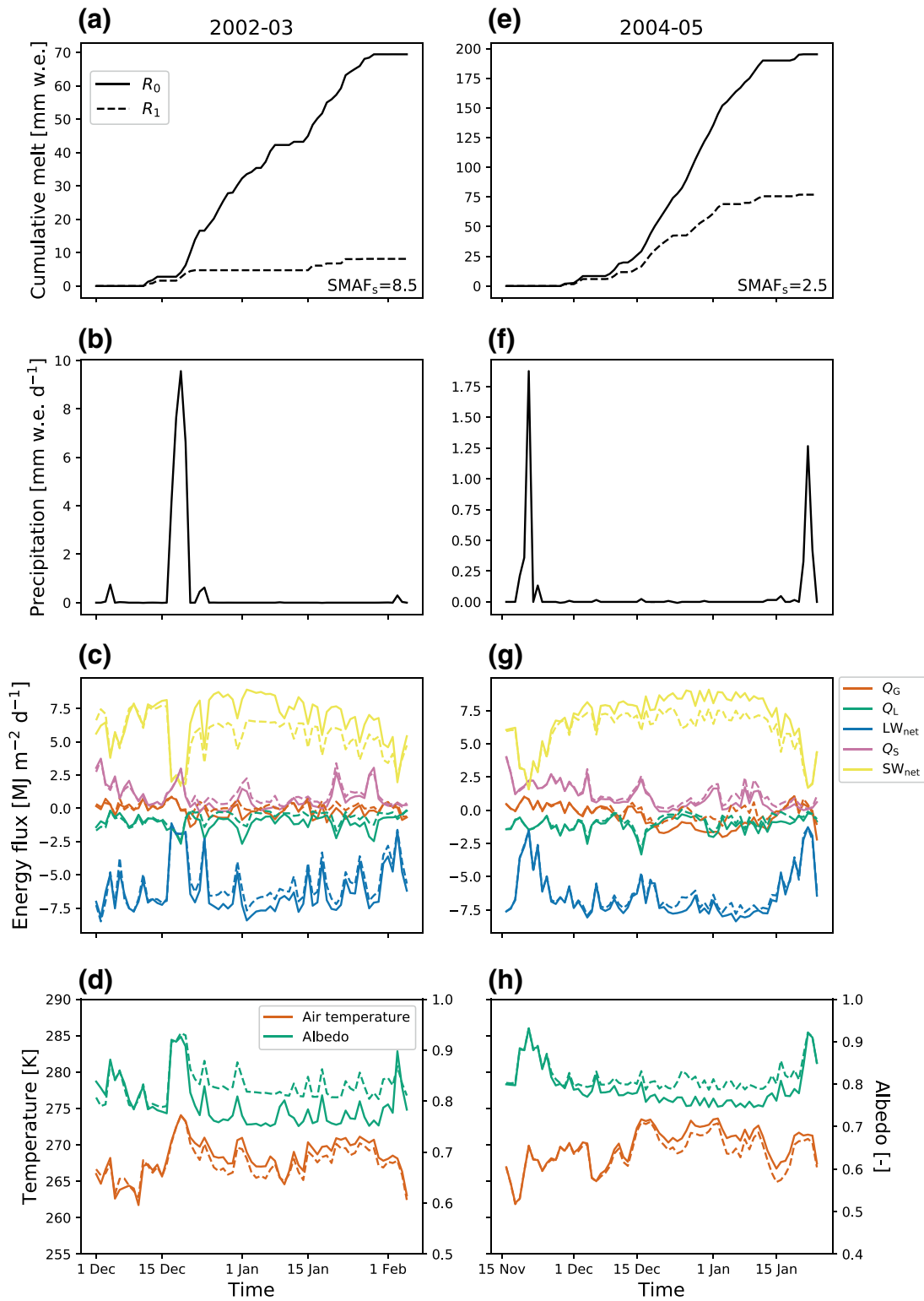


**Figure 6.** Time series of daily totals of (a, e) surface melt, (b, f) precipitation, (c, g) fluxes of surface energy balance components, and (d, h) average 2 m air temperature and surface albedo, during the summer of 2002–2003 (a)–(d) and 2004–2005 (e)–(h) at King Baudouin ice shelf, Dronning Maud Land, East Antarctica (see Figure 2c, indicated by B). In all panels, solid lines indicate  $R_0$  and dashed lines indicate  $R_1$ . Please note the different y-axis scales.

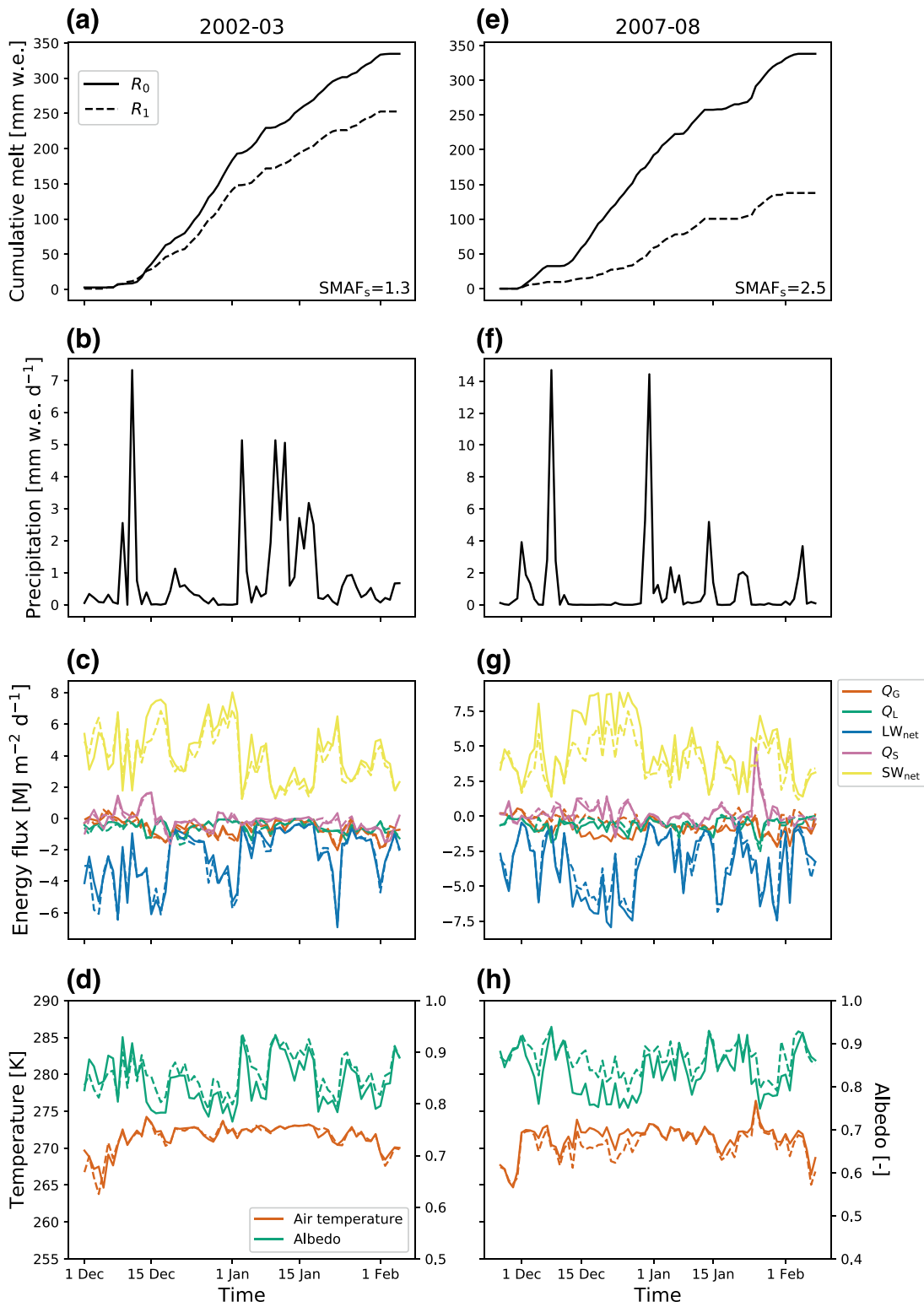


Figure 7. Same as Figure 6 for Larsen C ice shelf, Antarctic Peninsula (see Figure 2c, indicated by C).

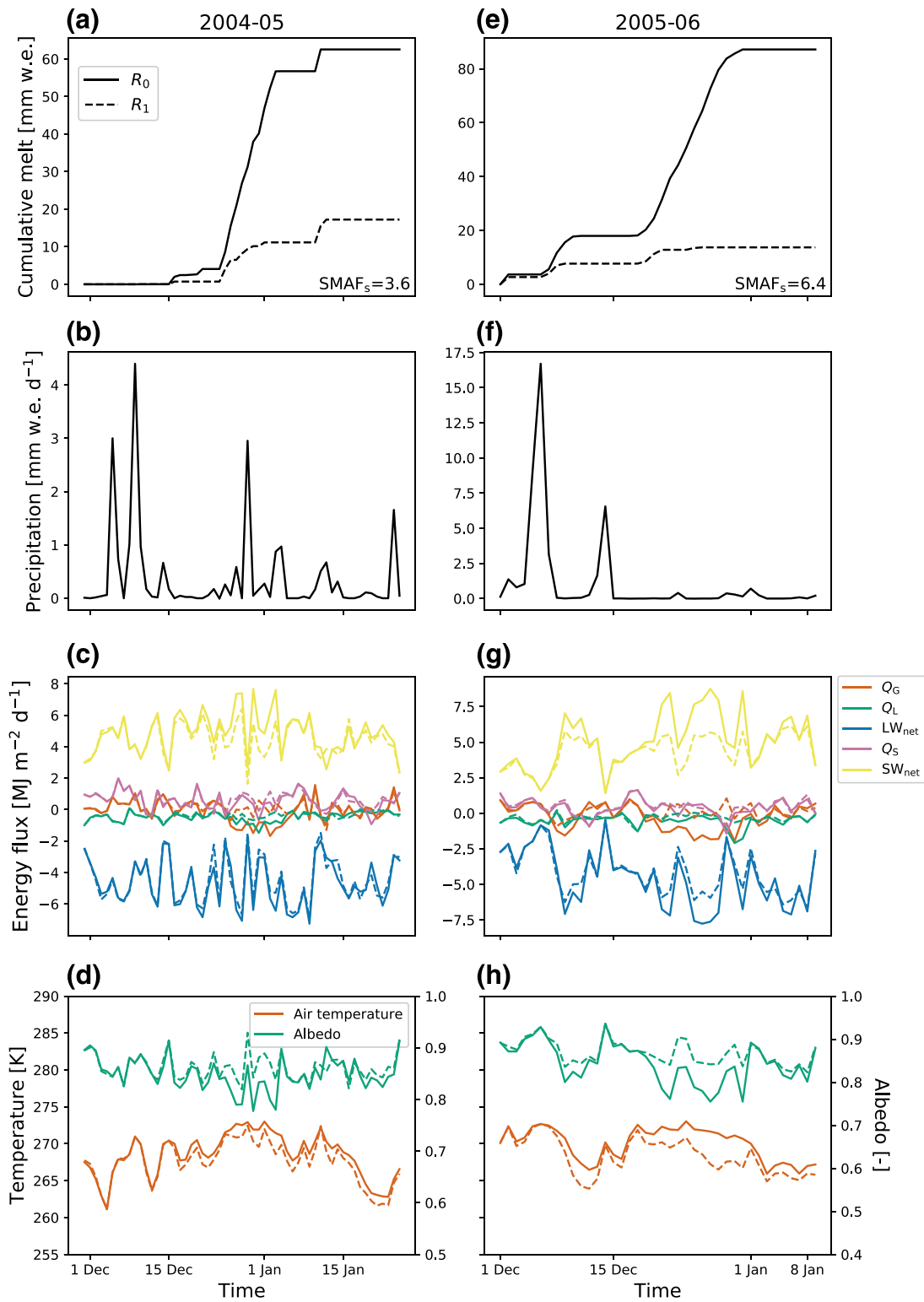


Figure 8. Same as Figure 6 for Amery ice shelf, Dronning Maud Land (see Figure 2c, indicated by A).

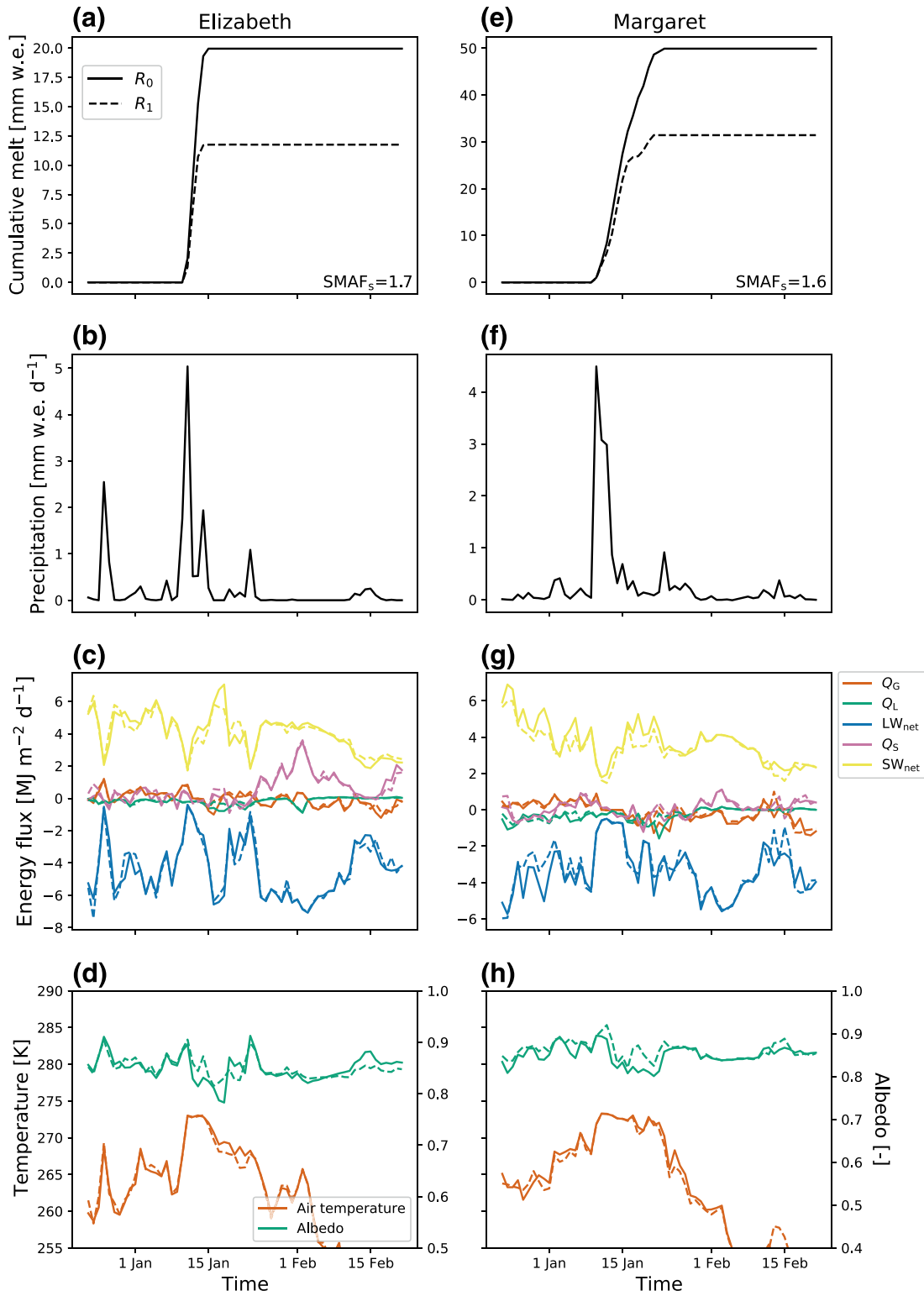


Figure 9. Same as Figure 6 for Elizabeth and Margaret stations (see Figure 2c).



“EZ” in Figure 2c). This season was strongly influenced by atmospheric rivers, advecting moist air to this part of the AIS, leading to unprecedented melt rates across the ice shelf and in West Antarctica (Nicolas et al., 2017). At these stations, temperatures are generally significantly lower than on King Baudouin ice shelf, but during the passage of the atmospheric river a melt episode is modeled at both Margaret and Elizabeth stations (Figure 9). Just before the melt event started, significant amounts of snow were deposited (Figures 9b and 9f), accompanied by small values of  $SW_{net}$  and  $LW_{net}$  (Figures 9c and 9g) and relatively high 2 m air temperatures (Figures 9d and 9h). Afterward, at Elizabeth station, melt was initiated by an increase in  $SW_{net}$ , resulting in significantly more melt in  $R_0$  than in  $R_1$ , similar to the melt events on King Baudouin ice shelf (Figure 6), and SMAF had a relatively large role in this melt event. Due to the quickly passing atmospheric rivers, 2 m air temperature dropped again and melt ceased. At Margaret station, there were overcast conditions during the first melt days, again indicated by small values of  $LW_{net}$  (Figure 9c), which resulted in a small role for SMAF as melt was primarily driven by enhanced downward long-wave radiation. After the passage of the atmospheric river,  $SW_{net}$  increased while 2 m air temperature remained high enough to accommodate surface melt. As a result, melt increased significantly in  $R_0$  whilst it remained low in  $R_1$ , displaying a significant role for SMAF.

These examples show the different meteorological circumstances that can lead to different SMAF values. The moderate-temperature regions have the highest  $SMAF_t$  values, because SMAF causes the albedo to be lowered sufficiently such that enhanced absorption of solar radiation causes continuous melt, which is absent in  $R_1$ . In warm regions, even in cases when the albedo is higher, melt continues in  $R_1$  (see Figure 7d). Finally, in cold regions, sustained melt does not occur because of the low temperatures. Melt is limited to single-day melt events instead, rendering SMAF unable to enhance surface melt for a prolonged period, resulting in small  $SMAF_s$  and  $SMAF_t$  values.

These examples illustrate that especially prolonged dry periods in temperate summer climates enable SMAF to greatly enhance summer melt amounts, due to the lack of snowfall resetting the surface albedo. Quantifying the correlation between dry periods and  $SMAF_s$  remains difficult. The exact timing of precipitation and early melt events is equally important: When dry snow metamorphism has already lowered the surface albedo before surface melt starts, SMAF is strongly reduced.

## 4. Discussion and Conclusions

### 4.1. SMAF in Antarctica

In this study, we investigate the spatial and temporal variability of the SMAF on the AIS. This is done by performing two simulations with the RACMO2, covering the period 1979–2018. This model uses a parameterization that relates the surface albedo to the grain size of snow; by disabling the contribution of refrozen snow to albedo lowering, this allows us to explicitly model the effect of SMAF on surface melt. One simulation is performed with the full albedo parameterization ( $R_0$ ), in the other simulation this refrozen-snow contribution is disabled ( $R_1$ ). Following Jakobs et al. (2019), we define SMAF as the ratio of cumulative surface melt between these two simulations, a value of 1 indicating no effect, a value of X indicating that melt is enhanced X-fold because of SMAF.

We find that SMAF is spatially highly variable on the AIS, ranging from values close to 1 in cold, low-melt regions such as the Ross and Filchner-Ronne ice shelves, to values up to 3 in coastal Dronning Maud Land (Figure 2). Relating  $SMAF_t$  to average summer (Nov–Feb) 2 m air temperature reveals a maximum around 265 K ( $T_c$ , Figure 4). This implies that the magnitude of the error made when ignoring SMAF will be largest when summer temperatures are close to this value. Many Antarctic ice shelves are located in the temperature regime where SMAF is currently optimal, except for the three largest ice shelves (Ross, Filchner-Ronne, and Amery), which are too cold, and the entire Antarctic Peninsula (Figure 5a), which is too warm.

Investigating the link between SMAF and the surface energy balance reveals that the timing of significant snowfall events with respect to surface melt is important. Seasonal SMAF is highest when melt occurs immediately after the last snowfall event at the onset of the melt season and in the absence of significant precipitation throughout the remainder of the season. The reason is that in this case, the surface albedo is not reset to the new-snow value and enhanced melt occurs continuously. When snowfall is not immediately

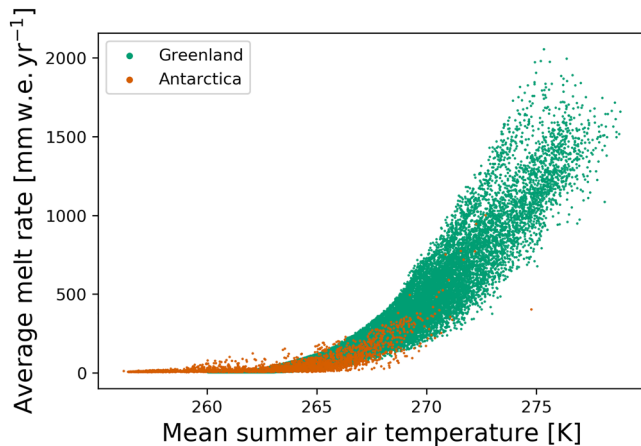


**Figure 10.** Period-average summer 2 m air temperature versus average seasonal surface melt for Greenland (green, accumulation zone only, Noël et al. (2018)) and Antarctica (orange) for all grid points with period-average seasonal surface melt of at least 5 mm w.e. Summer is defined as November–February in Antarctica and May–August in Greenland.

followed by surface melt, the surface albedo is lowered by dry snow metamorphism. The effect of refrozen snow on seasonal albedo is subsequently much smaller than in the previous example, and therefore SMAF is less important. On Larsen C ice shelf, located in the mild AP, the 2 m air temperature is normally high enough to facilitate near-continuous surface melt; SMAF does enhance surface melt but it does not determine whether surface melt continues or ceases. This is contrary to moderate-temperature locations, where SMAF can be the determining factor for the start and continuation of surface melt.

Although a large part of Antarctica is currently too cold for an optimal SMAF, which occurs at  $\sim 265$  K, rising temperatures in the future could expose even the largest ice shelves to a strong increase in surface melt because of SMAF.

#### 4.2. Outlook: Greenland and the Future

The shaded areas in Figure 4 indicate the normalized distributions of temperature for all grid points with period-average seasonal surface melt of at least 1 mm w.e. in Antarctica (orange) and in Greenland (green, accumulation zone only, Noël et al. (2018)). The Ross, Filchner-Ronne and Amery ice shelves correspond to the left peak of this distribution, where

the impact of SMAF on surface melt rates is limited (Section 3.3). The right peak of this temperature distribution represents the remaining ice shelves along East and West Antarctica. The higher temperatures are a result of their more northerly location than the Ross, Filchner-Ronne, and Amery ice shelves. This shows that in the current climate, the majority of melt points fall in a regime with moderate SMAF, with only few locations significantly above  $T_c$ .

In a warmer climate, the distributions in Figure 4 will shift toward the right. The East Antarctic ice shelves, located in the right peak of the orange distribution, will slowly become less affected by SMAF. On the other hand, the Ross, Filchner-Ronne, and Amery ice shelves, which are in the left peak of this distribution, will gradually be exposed to higher SMAF values. As SMAF will become more important on these ice shelves, surface melt will increase relatively more strongly in these regions than for example on coastal Dronning Maud Land ice shelves. This might negatively affect the stability of the ice shelves through processes such as increased firn saturation, increased ice temperatures and hydrofracturing, and therewith affects the future of the AIS (Trusel et al., 2015).

The temperature distribution of melt points in Greenland is shown in green shading in Figure 4 (accumulation zone only, Noël et al. (2018)). The absence of large, flat ice shelves results in large differences with the distribution of Antarctica. The bulk of the Greenland distribution is centered around 260 K, which represents the high and flat interior accumulation zone. Figure 10 shows the melt-temperature relation for Antarctica and Greenland (accumulation zone only), relating the period-average summer melt and summer temperature (November–February for Antarctica, May–August for Greenland). The Greenland curve seems to be an extension of the Antarctica curve, suggesting that when temperature increases in the southern hemisphere, the Antarctic melt climate will increasingly resemble the contemporary Greenland melt climate. Note also that the temperature-SMAF relationship (Figure 4) is not very sensitive to the time period for which it is calculated (not shown). This suggests that this relationship might also be applicable to Greenland. In order to assess how SMAF might affect surface melt in Greenland, we therefore apply the temperature-SMAF relationship to the Greenland temperature distribution.

Figure 5b shows that in Greenland, SMAF is active in a large part of the interior ice sheet in southern Greenland, and a narrow band in the middle-elevated accumulation zone around the rest of the ice sheet. In a warming climate, the SMAF region will migrate inland, corresponding to a right-ward shift of the green temperature distribution in Figure 4. This leads to a rapid increase of the area being affected by SMAF when

2 m air temperatures over Greenland continue to rise. These tentative results warrant a dedicated simulation covering the Greenland ice sheet to further investigate SMAF in Greenland.

## Data Availability Statement

The data are available on <https://doi.org/10.5281/zenodo.3836044>.

## Acknowledgments

This research has been supported by the Nederlandse Organisatie voor Wetenschappelijk Onderzoek (Grant no. 866.15.204). Michiel van den Broeke acknowledges support from the Netherlands Earth System Science Center (NESSC). This publication was supported by PROTECT. This project has received funding from the European Union's Horizon 2020 research and innovation program under grant agreement no. 869304, PROTECT contribution number 10. The authors thank Brice Noël for carrying out the RACMO2.3p2 Greenland simulation.

## References

- Agosta, C., Amory, C., Kittel, C., Orsi, A., Favier, V., Gallée, H., et al. (2019). Estimation of the Antarctic surface mass balance using the regional climate model MAR (1979–2015) and identification of dominant processes. *The Cryosphere*, *13*, 281–296. <https://doi.org/10.5194/tc-13-281-2012>
- Alexander, P. M., LeGrande, A. N., Fischer, E., Tedesco, M., Fettweis, X., Kelley, M., et al. (2019). Simulated Greenland surface mass balance in the GISS modelE2 GCM: Role of the ice sheet surface. *Journal of Geophysical Research: Earth Surface*, *124*, 750–765. <https://doi.org/10.1029/2018JF004772>
- Bindschadler, R., Choi, H., Wichlacz, A., Bingham, R., Bohlander, J., Brunt, K., et al. (2011). Getting around Antarctica: New high-resolution mappings of the grounded and freely-floating boundaries of the Antarctic ice sheet created for the International Polar Year. *The Cryosphere*, *5*, 569–588. <https://doi.org/10.5194/tc-5-569-2011>
- Bisiaux, M. M., Edwards, R., McConnell, J. R., Curran, M. A. J., Van Ommen, T. D., Smith, A. M., et al. (2012). Changes in black carbon deposition to Antarctica from two high-resolution ice core records, 1850–2000 AD. *Atmospheric Chemistry and Physics*, *12*, 4107–4115. <https://doi.org/10.5194/acp-12-4107-2012>
- Braun, M., Humbert, A., & Moll, A. (2009). Changes of Wilkins ice shelf over the past 15 years and inferences on its stability. *The Cryosphere*, *3*, 41–56. <https://doi.org/10.5194/tc-3-41-2009>
- Bromwich, D. H., Otieno, F. O., Hines, K. M., Manning, K. W., & Shilo, E. (2013). Comprehensive evaluation of polar weather research and forecasting model performance in the Antarctic. *Journal of Geophysical Research*, *118*, 274–292. <https://doi.org/10.1029/2012JD018139>
- Cullather, R. I., Nowicki, S. M. J., Zhao, B., & Suarez, M. J. (2014). Evaluation of the surface representation of the Greenland ice sheet in a general circulation model. *Journal of Climate*, *27*, 4835–4856. <https://doi.org/10.1175/JCLI-D-13-00635.1>
- ECMWF (2009). Part IV: Physical Processes. *Ips documentation cy33r1*. Author Retrieved from. <https://www.ecmwf.int/node/9227>
- Ettema, J., Van den Broeke, M. R., Van Meijgaard, E., Van de Berg, W. J., Box, J. E., & Steffen, K. (2010). Climate of the Greenland ice sheet using a high-resolution climate model – Part 1: Evaluation. *The Cryosphere*, *4*, 511–527. <https://doi.org/10.5194/tc-4-511-2010>
- Gardner, A. S., & Sharp, M. J. (2010). A review of snow and ice albedo and the development of a new physically based broadband albedo parameterization. *Journal of Geophysical Research*, *115*, F01009. <https://doi.org/10.1029/2009JF001444>
- Glasser, N. F., & Scambos, T. A. (2008). A structural glaciological analysis of the 2002 Larsen B ice-shelf collapse. *Journal of Glaciology*, *54*(184), 3–16. <https://doi.org/10.3189/002214308784409017>
- Grenfell, T. C., Warren, S. G., & Mullen, P. C. (1994). Reflection of solar radiation by the Antarctic snow surface at ultraviolet, visible, and near-infrared wavelengths. *Journal of Geophysical Research*, *99*(D9), 18669–18684. <https://doi.org/10.1029/94JD01484>
- Jakobs, C. L., Reijmer, C. H., Kuipers Munneke, P., König-Langlo, G., & Van den Broeke, M. R. (2019). Quantifying the snowmelt-albedo feedback at Neumayer Station, East Antarctica. *The Cryosphere*, *13*, 1473–1485. <https://doi.org/10.5194/tc-13-1473-2019>
- Jakobs, C. L., Reijmer, C. H., Smeets, C. J. P. P., Trusel, L. D., Van de Berg, W. J., Van den Broeke, M. R., et al. (2020). A benchmark dataset of in situ Antarctic surface melt rates and energy balance. *Journal of Glaciology*, *66*(256), 291–302. <https://doi.org/10.1017/jog.2020.6>
- Jonsell, U. Y., Navarro, F. J., Bañón, M., Lapazaran, J. J., & Otero, J. (2012). Sensitivity of a distributed temperature-radiation index melt model based on AWS observations and surface energy balance fluxes, Hurd Peninsula glaciers, Livingston Island, Antarctica. *The Cryosphere*, *6*, 539–552. <https://doi.org/10.5194/tc-6-539-2012>
- King, J. C., Gadian, A., Kirchgassner, A., Kuipers Munneke, P., Lachlan-Cope, T. A., Orr, A., et al. (2015). Validation of the summertime surface energy budget of Larsen C ice shelf (Antarctica) as represented in three high-resolution atmospheric models. *Journal of Geophysical Research: Atmosphere*, *120*, 1335–1347. <https://doi.org/10.1002/2014JD022604>
- Kingslake, J., Ely, J. C., Das, I., & Bell, R. E. (2017). Widespread movement of meltwater onto and across Antarctic ice shelves. *Nature*, *544*, 349–352. <https://doi.org/10.1038/nature22049>
- Kuipers Munneke, P., Van den Broeke, M. R., Lenaerts, J. T. M., Flanner, M. G., Gardner, A. S., & Van de Berg, W. J. (2011). A new albedo parameterization for use in climate models over the Antarctic ice sheet. *Journal of Geophysical Research*, *116*, D05114. <https://doi.org/10.1029/2010JD015113>
- Lenaerts, J. T. M., Lhermitte, S., Drews, R., Ligtenberg, S. R. M., Berger, S., Helm, V., et al. (2017). Meltwater produced by wind-albedo interaction stored in an East Antarctic ice shelf. *Nature Climate Change*, *7*, 58–62. <https://doi.org/10.1038/nclimate3180>
- Lenaerts, J. T. M., Ligtenberg, S. R. M., Medley, B., Van de Berg, W. J., Konrad, H., Nicolas, J. P., et al. (2018). Climate and surface mass balance of coastal West Antarctica resolved by regional climate modeling. *Annals of Glaciology*, *59*(76pt1), 29–41. <https://doi.org/10.1017/aog.2017.42>
- Lenaerts, J. T. M., Van den Broeke, M. R., Déry, S. J., Van Meijgaard, E., Van de Berg, W. J., Palm, S. P., et al. (2012). Modeling drifting snow in Antarctica with a regional climate model: 1. Methods and model evaluation. *Journal of Geophysical Research*, *117*, D05108. <https://doi.org/10.1029/2011JD016145>
- Marquetto, L., Kaspari, S., & Simões, J. C. (2020). Refractory black carbon (rBC) variability in a 47-year West Antarctic snow and firn core. *The Cryosphere*, *14*, 1537–1554. <https://doi.org/10.5194/tc-14-1537-2020>
- Massom, R. A., Scambos, T. A., Bennetts, L. G., Reid, P. A., Squire, V. A., & Stammerjohn, S. E. (2018). Antarctic ice shelf disintegration triggered by sea ice loss and ocean swell. *Nature*, *558*, 383–389. <https://doi.org/10.1038/s41586-018-0212-1>
- Morlighem, M., Rignot, E., Binder, T., Blankenship, D. D., Drews, R., Eagles, G., et al. (2020). Deep glacial troughs and stabilizing ridges unveiled beneath the margins of the Antarctic ice sheet. *Nature Geoscience*, *13*, 132–137. <https://doi.org/10.1038/s41561-019-0510-8>
- Nicolas, J., Vogelmann, A. M., Scott, R. C., Wilson, A. B., Cadetdu, M. P., Bromwich, D. H., et al. (2017). January 2016 extensive summer melt in West Antarctica favored by strong El Niño. *Nature Communications*, *8*, 15799. <https://doi.org/10.1038/ncomms15799>

- Noël, B. P. Y., Van de Berg, W. J., Van Wessem, J. M., Van Meijgaard, E., Van As, D., Lenaerts, J. T. M., et al. (2018). Modeling the climate and surface mass balance of polar ice sheets using RACMO2, part 1: Greenland (1958–2016). *The Cryosphere*, *12*, 811–831. <https://doi.org/10.5194/tc-12-811-2018>
- Padman, L., Costa, D. P., Dinniman, M. S., Fricker, H. A., Goebel, M. E., Huckstadt, L. A., et al. (2012). Oceanic controls on the mass balance of Wilkins ice shelf, Antarctica. *Journal of Geophysical Research*, *117*, C01010. <https://doi.org/10.1029/2011JC007301>
- Pritchard, H. D., Ligtenberg, S. R. M., Fricker, H. A., Vaughan, D. G., Van den Broeke, M. R., & Padman, L. (2012). Antarctic ice-sheet loss driven by basal melting of ice shelves. *Nature*, *484*, 502–505. <https://doi.org/10.1038/nature10968>
- Reijmer, C. H., Van Meijgaard, E., & Van den Broeke, M. R. (2005). Evaluation of temperature and wind over Antarctica in a Regional Atmospheric Climate Model using 1 year of automatic weather station data and upper air observations. *Journal of Geophysical Research*, *110*, D04103. <https://doi.org/10.1029/2004JD005234>
- Rott, H., Müller, F., Nagler, T., & Floricioiu, D. (2011). The imbalance of glaciers after disintegration of Larsen-B ice shelf, Antarctic Peninsula. *The Cryosphere*, *5*, 125–134. <https://doi.org/10.5194/tc-5-125-2011>
- Scambos, T. A., Bohlander, J. A., Shuman, C. A., & Skvarca, P. (2004). Glacier acceleration and thinning after ice shelf collapse in the Larsen B embayment, Antarctica. *Geophysical Research Letters*, *31*, L18402. <https://doi.org/10.1029/2004GL020670>
- Shepherd, A., Ivins, E. R., Rignot, E., Smith, B., Van den Broeke, M. R., Velicogna, I., et al. (2018). Mass balance of the Antarctic ice sheet from 1992 to 2017. *Nature*, *558*, 219–222. <https://doi.org/10.1038/s41586-018-0179-y>
- Souvereinjs, N., Gossart, A., Demuzere, M., Lenaerts, J. T. M., Medley, B., Gorodetskaya, I. V., et al. (2019). A new Regional Climate Model for POLAR-CORDEX: Evaluation of a 30-Year Hindcast with COSMO-CLM2 over Antarctica. *Journal of Geophysical Research: Atmosphere*, *124*, 1405–1427. <https://doi.org/10.1029/2018JD028862>
- Trusel, L. D., Frey, K. E., Das, S. B., Karnauskas, K. B., Kuipers Munneke, P., Van Meijgaard, E., et al. (2015). Divergent trajectories of Antarctic surface melt under two twenty-first-century climate scenarios. *Nature Geoscience*, *8*, 927–934. <https://doi.org/10.1038/NGEO2563>
- Turner, J., Orr, A., Gudmundsson, G. H., Jenkins, A., Bingham, R. G., Hillenbrand, C.-D., et al. (2017). Atmosphere-ocean-ice interactions in the Amundsen Sea Embayment, West Antarctica. *Reviews of Geophysics*, *55*, 235–276. <https://doi.org/10.1002/2016RG000532>
- Undén, P., Rontu, L., Järvinen, H., Lynch, P., Calvo, J., Cats, G., et al. (2002). *HIRLAM-5 scientific documentation [computer software manual]*. Retrieved from [http://hirlam.org/index.php/hirlam-documentation/doc\\_download/308-unden-et-al-2002](http://hirlam.org/index.php/hirlam-documentation/doc_download/308-unden-et-al-2002)
- Van Dalum, C. T., Van de Berg, W. J., Lhermitte, S., & Van den Broeke, M. R. (2020). Evaluation of a new snow albedo scheme for the Greenland ice sheet in the Regional Atmospheric Climate Model (RACMO2). *The Cryosphere*, *14*, 3645–3662. <https://doi.org/10.5194/tc-14-3645-2020>
- Van Dalum, C. T., Van de Berg, W. J., Libois, Q., Picard, G., & Van den Broeke, M. R. (2019). A module to convert spectral to narrowband snow albedo for use in climate models: SNOWBALL v1.2. *Geoscientific Model Development*, *12*, 5157–5175. <https://doi.org/10.5194/gmd-12-5157-2019>
- Van de Berg, W. J., & Medley, B. (2016). Brief Communication: Upper-air relaxation in RACMO2 significantly improved modeled inter-annual surface mass balance variability in Antarctica. *The Cryosphere*, *10*, 459–463. <https://doi.org/10.5194/tc-10-459-2016>
- Van den Broeke, M. R. (2005). Strong surface melting preceded collapse of Antarctic Peninsula ice shelf. *Geophysical Research Letters*, *32*, L12815. <https://doi.org/10.1029/2005GL023247>
- Van den Broeke, M. R., Reijmer, C. H., Van As, D., Van de Wal, R. S. W., & Oerlemans, J. (2005). Seasonal cycles of Antarctic surface energy balance from automatic weather stations. *Annals of Glaciology*, *41*, 131–139. <https://doi.org/10.3189/172756405781813168>
- Van den Broeke, M. R., Van As, D., Reijmer, C. H., & Van de Wal, R. S. W. (2005). Sensible heat exchange at the Antarctic snow surface: A study with automatic weather stations. *International Journal of Climatology*, *25*, 1081–1101. <https://doi.org/10.1002/joc.1152>
- Van Kampenhout, L., Lenaerts, J. T. M., Lipscomb, W. H., Sacks, W. J., Lawrence, D. M., Slater, A. G., et al. (2017). Improving the representation of polar snow and firn in the community earth system model. *Journal of Advances in Modeling Earth Systems*, *9*, 2583–2600. <https://doi.org/10.1002/2017MS000988>
- Van Wessem, J. M., Van de Berg, W. J., Noël, B. P. Y., Van Meijgaard, E., Birnbaum, G., Jakobs, C. L., et al. (2018). Modeling the climate and surface mass balance of polar ice sheets using RACMO2, Part 2: Antarctica (1979–2016). *The Cryosphere*, *12*, 1479–1498. <https://doi.org/10.5194/tc-12-1479-2018>
- Warren, S. G., & Clarke, A. D. (1990). Soot in the atmosphere and snow surface of Antarctica. *Journal of Geophysical Research*, *95*(D2), 1811–1816. <https://doi.org/10.1029/JD095iD02p01811>
- Wiesenekker, J. M., Kuipers Munneke, P., Van den Broeke, M. R., & Smeets, C. J. P. P. (2018). A multidecadal analysis of Föhn Winds over Larsen C ice shelf from a combination of observations and modeling. *Atmosphere*, *9*, 172. <https://doi.org/10.3390/atmos9050172>
- Wiscombe, W. J., & Warren, S. G. (1980). A model for the spectral albedo of snow. I: Pure snow. *Journal of the Atmospheric Sciences*, *37*, 2712–2733. [https://doi.org/10.1175/1520-0469\(1980\)037<2712:AMFTSA>2.0.CO;2](https://doi.org/10.1175/1520-0469(1980)037<2712:AMFTSA>2.0.CO;2)
- Wouters, B., Martín-Español, A., Helm, V., Flament, T., Van Wessem, J. M., Ligtenberg, S. R. M., et al. (2015). Dynamic thinning of glaciers on the Southern Antarctic Peninsula. *Science*, *348*(6237), 899–903. <https://doi.org/10.1126/science.aaa5727>